Journal of Ginseng Research 46 (2022) 771–779

Contents lists available at ScienceDirect

Journal of Ginseng Research

journal homepage: https://www.sciencedirect.com/journal/journal-of-ginseng-research

Research Article

Evaluation of 20(S)-ginsenoside Rg3 loaded hydrogel for the treatment of perianal ulcer in a rat model

Longhai Jin [a,1], Jinping Liu [b,1], Shu Wang [c,1], Linxian Zhao [d], Jiannan Li [d,*]

[a] Department of Radiology, The Second Hospital of Jilin University, Changchun, China
[b] Research Center of Natural Drug, School of Pharmaceutical Sciences, Jilin University, Changchun, China
[c] Department of Radiotherapy, The Second Hospital of Jilin University, Changchun, China
[d] Department of General Surgery, The Second Hospital of Jilin University, Changchun, China

ARTICLE INFO

Article history:
Received 2 October 2021
Received in revised form
2 March 2022
Accepted 8 March 2022
Available online 11 March 2022

Keywords:
Perianal ulcer
Hydrogel
20(S)-ginsenoside Rg3
Drug release
Wound healing

ABSTRACT

Background: As a kind of common complication of the surgery of perianal diseases, perianal ulcer is known as a nuisance. This study aims to develop a kind of 20(S)-ginsenoside Rg3 (Rg3)-loaded hydrogel to treat perianal ulcers in a rat model.

Methods: The copolymers $PLGA_{1600}$-PEG_{1000}-$PLGA_{1600}$ were synthesized by ring-opening polymerization process and Rg3-loaded hydrogel was then developed. The perianal ulcer rat model was established to analyze the treatment efficacy of Rg3-loaded hydrogel for ulceration healing for 15 days. The animals were divided into control group, hydrogel group, free Rg3 group, Rg3-loaded hydrogel group, and Lidocaine Gel® group. The residual wound area rate was calculated and the blood concentrations of interleukin-1 (IL-1), interleukin-6 (IL-6), and vascular endothelial growth factor (VEGF) were recorded. Hematoxylin and eosin (H&E) staining, Masson's Trichrome (MT) staining, and tumor necrosis factor α (TNF-α), Ki-67, CD31, ERK1/2, and NF-κB immunohistochemical staining were performed.

Results: The biodegradable and biocompatible hydrogel carries a homogenous interactive porous structure with 10 μm pore size and five weeks in vivo degradation time. The loaded Rg3 can be released sustainably. The in vitro cytotoxicity study showed that the hydrogel had no effect on survival rate of murine skin fibroblasts L929. The Rg3-loaded hydrogel can facilitate perianal ulcer healing by inhibiting local and systematic inflammatory responses, swelling the proliferation of nuclear cells, collagen deposition, and vascularization, and activating ERK signal pathway.

Conclusion: The Rg3-loaded hydrogel shows the best treatment efficacy of perianal ulcer and may be a candidate for perianal ulcer treatment.

1. Introduction

As an essential barrier tissue of the human body, skin consisting of the epidermis, dermis, and subcutaneous tissue can maintain the internal environment and prevent microorganism invasion with its immune protection and repair capabilities [1,2]. Open wounds, common in human skin, impair the dermis and subcutaneous tissues, like blood vessels, muscles and nerves [3]. Skin barrier defects that occur after trauma can cause many local and systemic problems [3]. When skin tissue is injured, our body will start the wound healing process. If the acute skin injury is not repaired typically, it will form a chronic, non-healing wound or form hyperplastic scar tissue [4,5]. Serious perianal inflammation and edema is always associated with hemorrhoid surgery, and often results in delayed wound or perianal ulcer [6] that can be easily contaminated by the perianal exudates with difficult ulcer healing [7].

Biological dressings are commonly used clinically to cover wounds to temporarily replace the barrier function of the skin [1,8]. The ideal biological dressing should have the following properties: (1) Physical properties like breathability, moisture retention, mechanical stability, wound adhesion, and the ability to absorb wound exudate [9,10]. (2) Biological properties like biological safety, biocompatibility, antibacterial properties, degradability, hemostasis, and the ability to promote wound healing and inhibit scar formation [9,10]. Traditional gauzes with satisfactory water absorption

* Corresponding author. The Second Hospital of Jilin University, Department of General Surgery, Changchun 130041, Jilin, China.
E-mail address: jnli@ciac.ac.cn (J. Li).
[1] These authors contributed equally to this work.

https://doi.org/10.1016/j.jgr.2022.03.002

ability, simple production process, low price fail to maintain wound moistness and curb bacterial growth, endangering delayed healing. Autologous or allogeneic tissue coverings resemble normal skin in its structure and collagen content with high cost and laborious sterilization and storage [10]. Synthetic dressings based on polymer materials have favorable air permeability and wound absorption capacity, but are susceptible to bacterial contamination [11]. Severe bacterial contamination always leaves further local inflammation, obstructs epithelial tissue repairment and neovascularization, causing delayed wound healing [12]. It is meaningful to turn up an original approach to prod strenuous perianal ulcer healing caused by the contaminated wounds.

With announced anti-inflammation and anti-oxidation effects, 20(S)-ginsenoside Rg3 (Rg3), one of the effective active ingredients of ginseng [13] has manifested the treatment efficacy of various diseases, like gastric ulcer [14], various cancers [15,16], and neurodegenerative defects [13]. Likewise, as a traditional Chinese medicine, Rg3 is deemed safe in vivo with fewer minor side effects to major organs. Rg3 has been applied for the treatment of wound healing by local injection or sustained release from electrospun fibers to the wound area and has shown promising potential for wound healing and hypertrophic scars formation [17,18]. Having been applied in wound healing in many studies, polymer-based hydrogel with certain pore size, can provide an enabling moist environment for cell proliferation and migration on wound surface while preventing bacteria invasion and avoiding the secondary infection of the wound surface. Moreover, its biocompatibility and biodegradability guarantee the safety of use. Therefore, polymer-based hydrogel and Rg3 integration may provide a different treatment method for perianal wound healing.

In this study, a kind of mPEG-b-PLGA hydrogel (H) loaded with Rg3 (H-Rg3) for perianal ulcer healing was developed in a rat model. The porous structure of the biocompatible and biodegradable hydrogel makes for oxygen transportation, the interaction of nutrients and other molecules as well as maintaining of the humid microenvironment. Rg3 can be slowly and locally released from the hydrogel to the wounds to perform anti-inflammation and angiogenesis effect. Our study aimed to combine the advantages of hydrogel and Rg3 for treating perianal ulcers. The synthesized H-Rg3 can significantly decrease the inflammatory responses, increase neovascularization and collagen deposition, and activate ERK signal pathway, promoting the healing of perianal ulcers in a rat model. Our study indicates that H-Rg3 may be promising for treating skin injury, even the perianal ulcer.

2. Materials and methods

2.1. Materials

Methoxy poly (ethylene glycol) (PEG; number average molecular weight (Mn) = 1500 g/mol), DL-lactide (D, L-LA), and glycolide (GA) were bought from Sigma-Aldrich (Shanghai, P.R. China). The 20(S)-ginsenoside Rg3 was obtained from Bioss Co., Ltd. (Beijing, P.R. China). Stannous octoate ($Sn(Oct)_2$) was acquired from Nanjing Reagent Co., Ltd. (Nanjing, P.R. China). Glacial acetic acid was purchased from Fujia Chemical Co., Ltd. (Zhengzhou, P.R. China). Elastase and Tween-80 used for drug release test were bought from Sigma-Aldrich (Shanghai, P.R. China). Mouse Elisa Kits interleukin-1 (IL-1), interleukin-6 (IL-6), and vascular endothelial growth factor (VEGF) were bought from Beyotime Biological Technology Co., Ltd. (Shanghai, P.R. China). The antibodies of tumor necrosis factor α (TNF-α), Ki-67, CD31, ERK1/2, and NF-κB were purchased from Abcam (Cambridge, USA).

2.2. Preparation and characterizations of mPEG-b-PLGA

Under the protection of Nitrogen and the catalysis of $Sn(Oct)_2$, mPEG-b-PLGA copolymer was obtained by ring-opening polymerization of D, L-LA and GA with PEG (Mn = 1000 g/mol) as the macro-initiator. The initial product is fully dissolved in distilled water at 4 °C, and then heated to 80 °C to precipitate. Then the product was freeze-dried to remove the excess water and the final mPEG-b-PLGA copolymer was obtained. The characterizations of mPEG-b-PLGA were analyzed by proton nuclear magnetic resonance (^{1}H NMR) on a 400 MHz Bruker spectrometer.

2.3. Preparation and characterizations of H-Rg3

The mPEG-b-PLGA copolymer was dissolved in phosphate buffer saline (Phosphate Buffer Solution, PBS, pH = 7.4) at a concentration of 30 wt% to obtain mPEG-b-PLGA hydrogel. The hydrogel is in the liquid phase at 4 °C and becomes solid at room temperature. Then, the hydrogel and Rg3 were dissolved in PBS (pH = 7.4) at 4 °C to obtain H-Rg3 with the Rg3 concentration of 10 wt%. The morphology of H-Rg3 was analyzed by scanning electron microscope (SEM; JEOL, JSM-7500F).

2.4. In vivo degradation

In the in vivo degradation study, the rats (n = 15) were injected subcutaneously 500 mg H or H-Rg3 by syringe (1 mL) with hydrogel turning solid and degraded continuously. The calculation of hydrogel weight loss is as followed, Weight loss (%) = $(W_0 - W_t)/W_0 \times 100\%$, where W_0 and W_t represent the initial weight and remaining weight at pre-set time points (1, 2, 3, 4, and 5 weeks) of the hydrogel, respectively. In detail, 3 rats were sacrificed at each time point for hydrogel degradation analysis.

2.5. Drug release test

H-Rg3 was cut into a 1.0 cm × 1.0 cm sized sample about 500 mg and was immersed in the 2.0 mL PBS (pH 7.4) solution containing 0.02 mg/mL elastase or 0.05% Tween-80. The solvent, placed in a shaker at 50 r/min and 37 °C, was collected for further detection and replaced with fresh ones daily. The amount of released Rg3 in different solutions was determined by ultraviolet/visible (UV/vis) absorbance at 254 nm and calculated through standard curves based on a series of concentrations of Rg3.

2.6. In vitro cytotoxicity

In vitro cytotoxicity of H-Rg3, H, and free Rg3 towards murine skin fibroblasts L929 was evaluated by MTT assay. Samples of H-Rg3 (mPEG-b-PLGA, 30 wt%), free Rg3, and H for in vitro cytotoxicity study were prepared at different Rg3 concentrations (2.5 wt%, 5 wt %, 10 wt%, 20 wt%, and 40 wt%) or collagen concentrations (2.5 wt%, 5 wt%, 10 wt%, 20 wt%, and 40 wt%). The cells were seeded in 96-well plates with 5×10^3 cells in each well, and cultured at 37 °C, 5% CO_2 for 24 h. Then the culture medium was replaced by 100 μL sample solutions at different concentrations at 37 °C, 5% CO_2 for 48 h, followed by adding 20 μL MTT reagent (5 mg/mL). After incubation at 37 °C for another 4 h, the medium was replaced by 100 μL DMSO. Finally, the OD values were analyzed by UV/vis at 490 nm. The medium-treated cells were served as controls and the cell viability was calculated based on the absorbance values.

2.7. In vivo perianal ulcer study

Female Wistar rats (180–220 g) were obtained from the Laboratory Animal Center of Jilin University. The animal study was approved by the Ethics Committee of the Animal Center of Jilin University. After 24 h fast, the rats were anesthetized with 7% chloral hydrate (0.5 mL/100 g) through intraperitoneal injection. The perianal skin of rats was sterilized and rats were fixed in a supine position. The perianal ulcer rat model was established by subcutaneously injecting glacial acetic acid (30 μL, 75%) to the perianal area at 3 points. Perianal ulceration with redness and inflammation exudation was formed about 48 h later. The animals were randomly divided into 5 groups with 8 animals in each one. Group 1 was treated with PBS solution daily as negative control; Group 2 was treated with H (about 500 mg) on the surface of the ulceration area; Group 3, wounds were uniformly injected with Rg3 solution (0.5 mL, 20 mg/mL) at 0, 3, 6, 9, and 12 days; Group 4 was treated with H-Rg3 (about 500 mg) on the surface of the ulceration area; Group 5, Lidocaine Gel® (about 500 mg) was used to cover the ulceration area evenly as positive control.

The basic vital signs of rats, such as the mental state, were recorded daily. The perianal ulcer of each animal was photographed daily and the residual wound area rate was calculated as $S_n/S_0 \times 100\%$. At 6 days and 15 days post treatment, 4 animals were randomly selected in each group and were euthanized, respectively. Before the euthanasia of each animal, blood samples were collected from the heart with serum from centrifugation at 2000 rpm for 15 min. The ulceration area of each animal was dissected. Levels of IL-1, IL-6, and VEGF in blood were analyzed using ELISA Kits.

2.8. Histopathological study

The ulceration tissues were rinsed with PBS, fixed in 4% (W/V) PBS-buffered paraformaldehyde, and finally embedded in paraffin. The tissues were sectioned at 5 μm serially and stained with hematoxylin and eosin (H&E). The inflammatory cells were counted under 100× magnification by three randomly selected pathologists. Masson's Trichrome (MT), TNF-α, Ki-67, CD31, ERK1/2, and NF-κB immunohistochemical staining were also performed. The MT images was analyzed by Image J Software (National Institutes of Health, Bethesda, MD, USA) and the blue channel was used to analyze the collagen fibers. For TNF-α, Ki-67, CD31, ERK1/2, and NF-κB immunohistochemical staining, the positive cells were stained brown-yellow, and the relative positive area was analyzed by Image J (National Institutes of Health, Bethesda, Maryland, USA).

2.9. Statistical analysis

Statistical analysis was performed by GraphPad Prism 7.0 (GraphPad Inc. San Diego, CA). Data were presented as mean ± standard derivation (SD). One-way ANOVA was used for comparison across multiple unpaired data and Student's t-test was used for comparison between two unpaired data. $*P < 0.05$ was described as statistical significance, and $**P < 0.01$ and $***P < 0.001$ were set as highly statistical significance.

3. Results

In this study, mPEG-b-PLGA copolymer was developed by ring-opening polymerization of D, L-LA and GA with PEG (Mn = 1000 g/mol) as the macro-initiator, which could be confirmed by ^{1}H NMR analysis (Fig. 1A). The feeding ratio of LA/GA is 3/1 and the final product is $PLGA_{1600}$-PEG_{1000}-$PLGA_{1600}$. The peaks (a, b, c, d, and e) in Fig. 1A represent the hydrogen atoms of different positions (shown in the structural formula) of mPEG-b-PLGA, the concentration of which being 30 wt%. The optical images of the gelation process are shown in Fig. 1B. The mPEG-b-PLGA hydrogel is in the liquid phase at 4 °C, comes to gel phase at 36 °C, and precipitates at 60 °C (Fig. 1B). The hydrogel analyzed by SEM (Fig. 1C) in its morphology and internal structure, exhibits a homogenous interactive porous structure with a pore size of ~10 μm. The sol-gel transition of the hydrogel in different concentrations towards temperature changes is shown in Fig. 1D. For specific concentration,

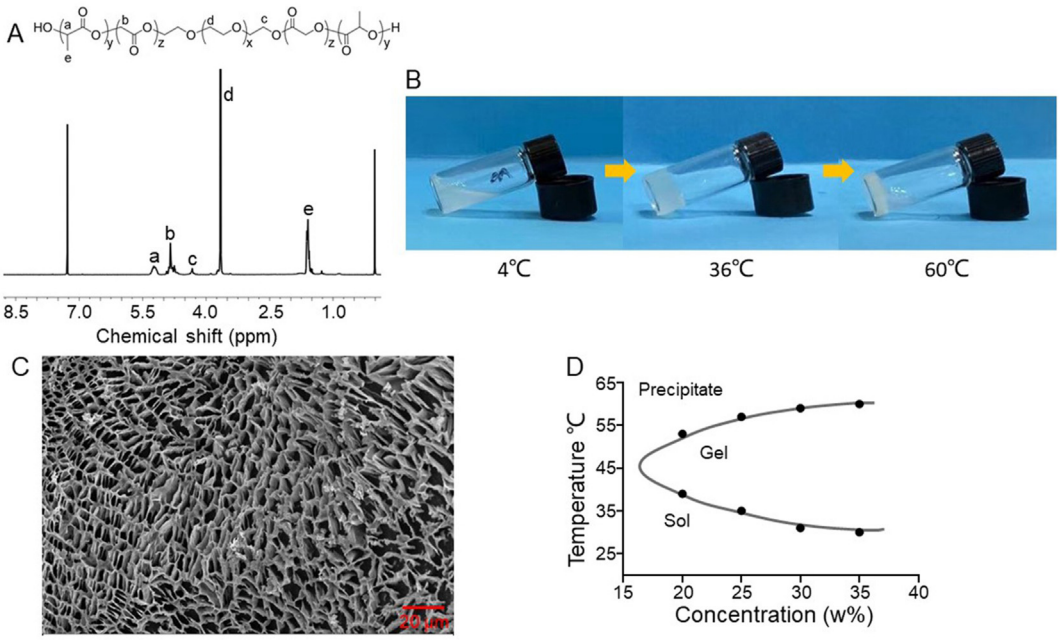

Fig. 1. Characteristics of mPEG-b-PLGA and Rg3-loaded hydrogel. (A) ^{1}H NMR analysis of mPEG-b-PLGA copolymer. (B) The optical images of gelation process of mPEG-b-PLGA hydrogel (30 wt%). (C) SEM analysis of Rg3-loaded hydrogel. (D) The sol-gel transition of the hydrogel in different concentrations towards temperature changes.

when temperatures are below, above, or in the middle of the curve, the gel is in different formations. For example, the hydrogel used in our study (30 wt%) is in gel formation at about 30 °C-60 °C.

The degradation study was performed by implanting hydrogel subcutaneously in rats. At pre-set time points post-implantation, the rats were euthanized and the degraded hydrogel was photographed and weighted. Fig. 2A shows that the gel degraded gradually with only a little remaining left at 5th-week post implantation. The weight remaining curve indicates the degradation profile of hydrogel (Fig. 2A). In addition, any signs of tissue edema or inflammatory responses around the degraded hydrogel in vivo were not found. For drug release study, massive Rg3 was released at the first 48 h, followed by a slow and constant release profile (Fig. 2B) in both groups. At 120 h, the released Rg3 was more in Elastase group (90.2 ± 4.1%) than that in PBS one (63.1 ± 6.0%, $***P < 0.001$). Fig. 2C shows the cytotoxicity study of H-Rg3 and free Rg3 towards murine skin fibroblasts L929. The cell viability was in a high state in all Rg3 concentrations groups and its viability was over 80%, even when the Rg3 concentration recorded 40 wt%. Furthermore, there was no difference in cell viability in H-Rg3 and free Rg3 groups towards diverse Rg3 concentrations. Fig. 2D indicates that the cell viability registered more than 90% at disparate collagen concentrations in H-Rg3 and H groups. There were also no momentous discrepancies in cell viability in both groups.

To evaluate the treatment efficacy of H-Rg3 towards perianal ulcer, the rat model was developed by subcutaneously injecting glacial acetic acid (30 μL, 75%) to the perianal area at 3 points. About 24 h later, perianal redness, edema, and inflammation could be found and perianal ulcer formed at about 48 h later. Then, the animals were divided into five groups and treated with PBS solution, H, free Rg3, H-Rg3, and Lidocaine Gel®, respectively. The animals were fed in a clean and ventilated experiment and under careful human care. During the animal study process, all the animals presented with a pretty favorable state without obvious signs of inappetence or weight loss. To record the healing of perianal ulcer, the images of ulceration were photographed at different time points and the residual wound area rate was calculated. Fig. 3A shows the images of the healing of ulceration in different groups at pre-set time points. At 3 days post treatment, the ulceration contracted obviously in H-Rg3 and Lidocaine groups and slightly in free Rg3 group, but didn't shrink in another two groups. The perianal tissue edema and redness were observed even at 9 days in Control, H, and free Rg3 groups with tissue edema vanished at 6 days in H-Rg3 and Lidocaine groups. At 15 days post treatment, the ulceration almost disappeared in H-Rg3 and Lidocaine groups, but mild ulceration can be found in H and free Rg3 groups and obvious ulceration can be found in Control group. The residual wound area rate was recorded and shown in Fig. 3B. At 15 days, the residual wound area rates were lower than 10% in H-Rg3 and Lidocaine groups without essential distinctions between them. The residual wound area rate was statistically smaller in H group than in Control group ($***P < 0.001$). Moreover, momentous inequality was

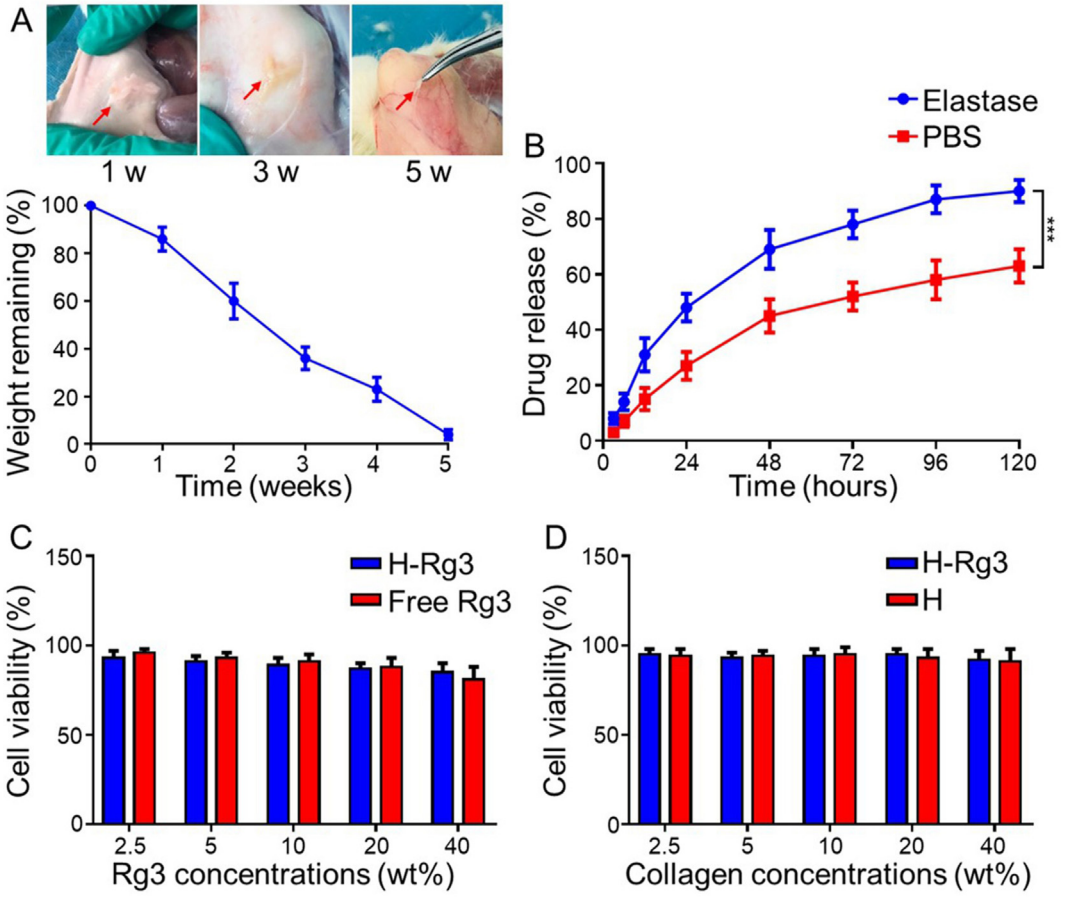

Fig. 2. Degradation, drug release, and in vitro cytotoxicity analysis. (A) In vivo degradation images of mPEG-b-PLGA hydrogel and the weight remaining at different time points. Red arrows indicate the degraded hydrogel at pre-set time. (B) Rg3 release profiles from the hydrogel immersed in elastase and PBS solutions. (C) In vitro cytotoxicity of H-Rg3 and free Rg3 at different Rg3 concentrations. (D) In vitro cytotoxicity of H-Rg3 and H at different collagen concentrations.

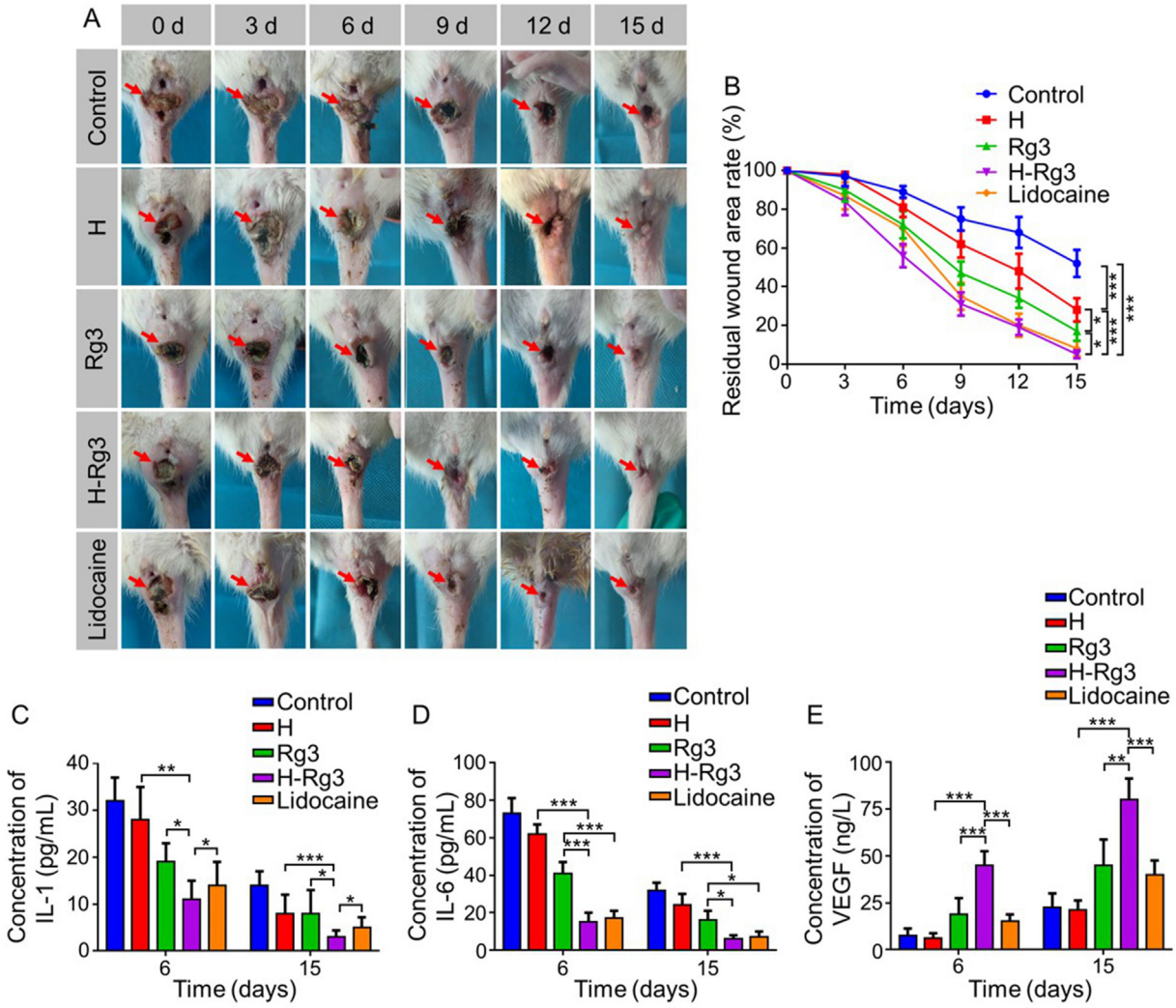

Fig. 3. Treatment effects of PBS, H, free Rg3, H-Rg3, and Lidocaine on the healing of perianal ulcer. (A) Represented images of perianal ulcer (red arrows) in different groups at preset time points. (B) Residual wound area rate of different groups. Blood concentrations of (C) IL-1, (D) IL-6, and (E) VEGF.

unveiled in the residual wound area rate between H-Rg3 group and free Rg3 group (*$P < 0.05$), or H group (***$P < 0.001$) or Control group (***$P < 0.001$). The blood concentrations of IL-1 and IL-6 were analyzed by ELISA method. For IL-1, H-Rg3 group showed the lowest value compared with the other four groups at 6 days and 15 days (Fig. 3C). Importantly, there was a statistically difference in IL-1 concentration between H-Rg3 and Lidocaine groups (*$P < 0.05$). For IL-6, H-Rg3 and Lidocaine groups showed the lowest level compared with other groups at 6 days and 15 days (Fig. 3D). There was no significant difference in IL-6 between H-Rg3 and Lidocaine groups. In addition, free Rg3 group showed more blood IL-6 levels than Lidocaine group at 6 days and 15 days (Fig. 3D). Fig. 3E shows that blood VEGF values of H-Rg3 group were the highest among all the groups at 6 days and 15 days. Moreover, a significant discrepancy was observed between H-Rg3 and Lidocaine groups (***$P < 0.001$) at 6 days and 15 days.

Fig. 4A shows the hematoxylin and eosin (H&E) staining of perianal ulcer tissues in different groups. At 6 days after treatment, the ulcers were still severe in Control and H groups, especially in Control one. The ulcer was serious and some local ulcer areas had penetrated into the muscular layer in Control group. In addition, large amounts of inflammatory cells and necrosis tissues have been spied. In H and free Rg3 groups, more inflammatory cells (compared with H-Rg3 group) and some necrosis tissues could be observed in ulcer tissues. However, the healing process has begun in H-Rg3 and Lidocaine groups with the formation of fibrous tissue. At 6 days post treatment, the ulcer could be discerned with slight inflammatory cells and fibrous tissue formation, hinting the initiation of the healing process in H-Rg3 and Lidocaine groups. At 15 days post treatment, the ulcer area was still apparent with inflammatory cells infiltration and some parts of necrosis tissues in Control group. In H and free Rg3 groups, the ulcers were in the early stage of the healing process with bits of angiogenesis and fibrous tissue formation. The perianal ulcer healed well with abundant fibrous tissues and angiogenesis in H-Rg3 group and Lidocaine group. Fig. 4B shows the inflammatory cells count in the ulcer area. At 6 days and 15 days after treatment, H-Rg3 group displays the most local inflammation inhibition effect compared with all the other four groups. Notably, there was a significant difference in the inflammatory cell count between H-Rg3 group and Lidocaine group (*$P < 0.05$) or free Rg3 group (***$P < 0.001$).

The collagen deposition was assessed by Masson staining of the perianal ulcer tissues. At 6 days after treatment, we could detect some collagen depositions in H-Rg3 group, but not obvious in the other four groups (Fig. 4C). At 15 days after treatment, plentiful depositions could be observed in H-Rg3 group. Some parts of

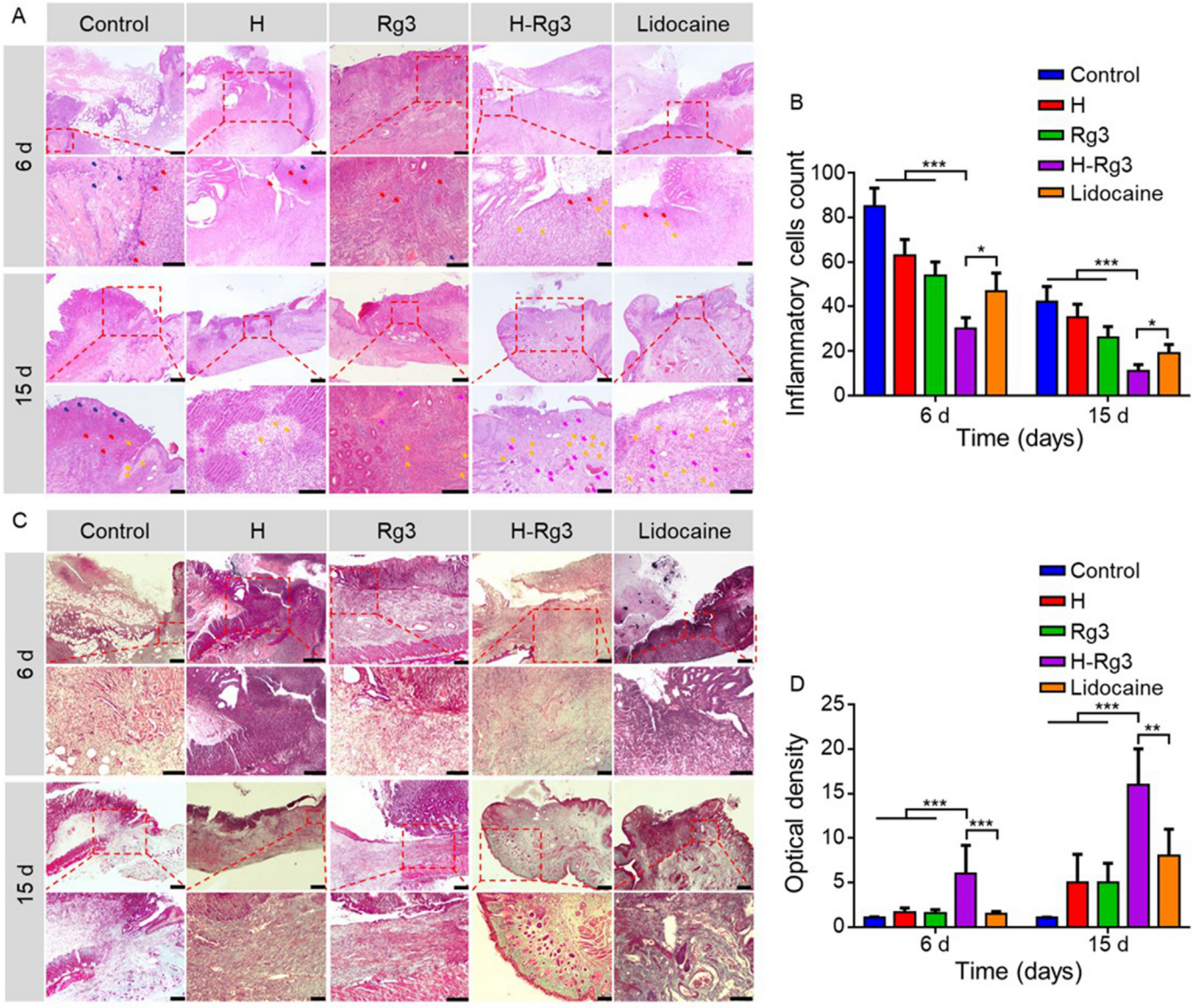

Fig. 4. H&E and Masson staining of perianal ulcers in different groups at 6 days and 15 days after treatment. (A) H&E staining of perianal ulcer tissues. Red, yellow, blue, and pink arrows show the inflammatory cells, fibrous tissues, necrosis tissues, and angiogenesis, respectively. (B) Inflammatory cells count in the ulcer area. (C) Masson staining of perianal ulcer tissues. (D) Semiquantitative analysis of collagen deposition. Scale bars = 200 μm.

ulceration area were stained slightly blue in H, free Rg3, and Lidocaine groups, indicating a few collagen depositions. Fig. 4D shows the semiquantitative analysis of collagen deposition in different groups. At 6 days after treatment, H-Rg3 showed the most abundant collagen depositions compared with the other four groups. Fifteen days witnessed massive depositions in H-Rg3 group, far more than others. In detail, there was a significant difference between H-Rg3 and Lidocaine (**$P < 0.01$) or free Rg3 groups (***$P < 0.001$).

TNF-α was highly expressed in Control and H groups at 6 days post treatment (Fig. 5A and B). At 15 days post treatment, the yellow-brown area was obvious in Control group. At 6 days and 15 days post treatment, H-Rg3 group exhibited less TNF-α expression compared with Control, H, and free Rg3 groups (Fig. 5B). However, there was no statistical difference between H-Rg3 and Lidocaine groups in TNF-α expression. At 15 days after treatment, TNF-α expression was less in H group than that in Control group (**$P < 0.01$). The expressions of Ki-67 and CD31 were the highest in H-Rg3 group than that in other groups at 6 days and 15 days after treatment (Fig. 5A, C, and D). In addition, there was significant difference between H-Rg3 and Lidocaine groups in the relative positive area of Ki-67 and CD31 (Fig. 5A, C, and D). As for ERK1/2 and NF-κB analysis, H-Rg3 showed the most ERK1/2 promotion and NF-κB inhibition effects compared with other groups (Fig. 5E and F), respectively. Notably, there was significant difference in ERK1/2 expression between H-Rg3 and Lidocaine (*$P < 0.05$) or free Rg3 groups (*$P < 0.05$) at 6 days and 15 days post treatment. At 6 days, both H-Rg3 and Lidocaine groups showed less NF-κB expressions compared with other groups, but there was no statistical difference between these two groups. At 15 days, the relative positive area of NF-κB was smaller in H-Rg3 group than that in all the other groups.

4. Discussion

In this study, Rg3-loaded mPEG-b-PLGA hydrogel was successfully prepared for the healing of perianal ulcers in a rat model. The

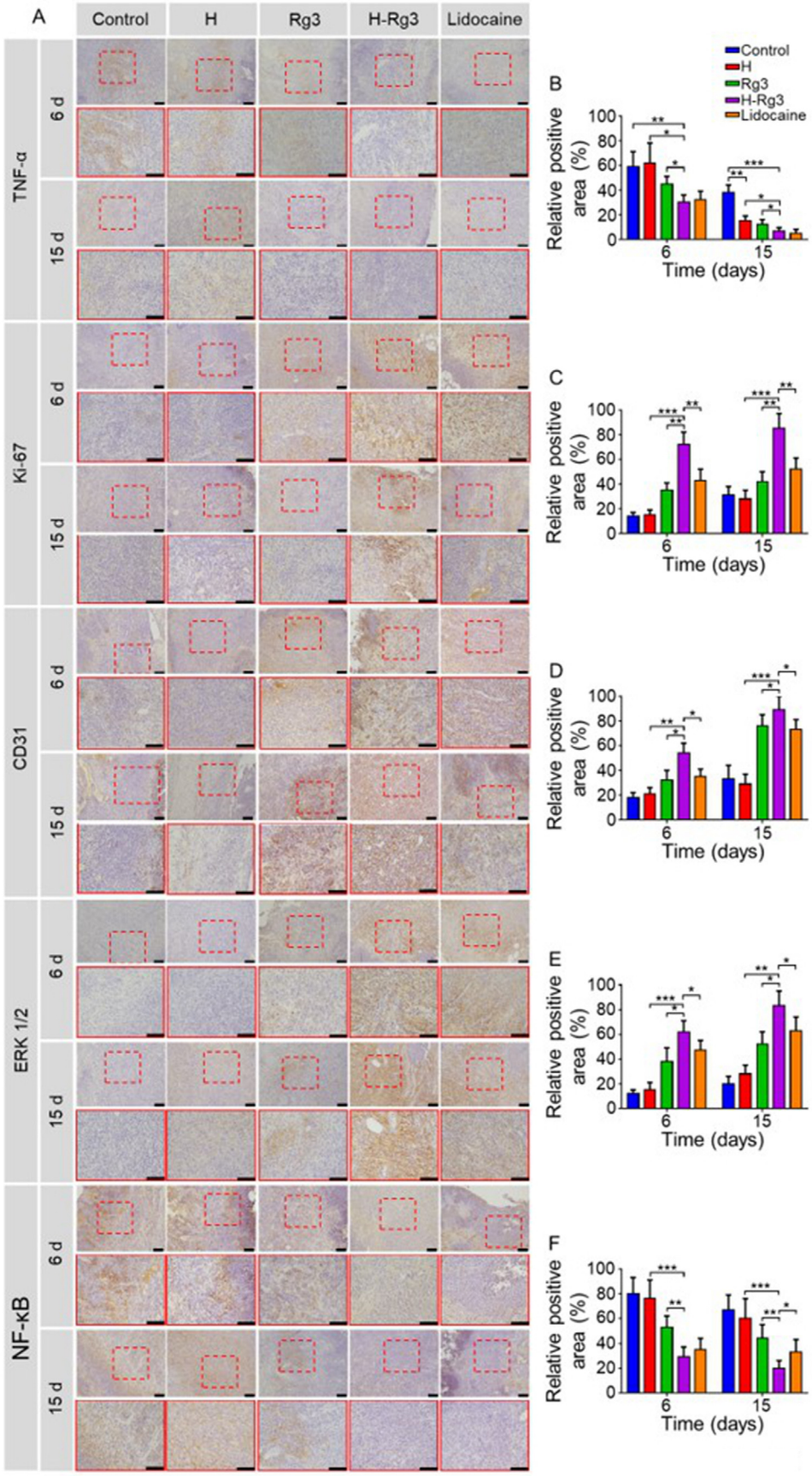
A
Control
H
Rg3
H-Rg3
Lidocaine
TNF-α
Ki-67
CD31
ERK 1/2
NF-κB
6 d
15 d
B
C
D
E
F
Control
H
Rg3
H-Rg3
Lidocaine
Relative positive area (%)
Time (days)
6
15

hydrogel is biocompatible and biodegradable with a porous structure. Rg3 can be released slowly to decrease the inflammatory responses, increase the neovascularization and collagen deposition, and activate the ERK signal pathway in the ulcer area. The structure and size fuel seeded cells communication, diffusion of the water molecule and other healing-conducive products, and initiate the internal transport of oxygen and nutrients [19,20]. The hydrogel used in this study possesses a homogenous interactive porous structure which benefits its wound healing effect. Besides, the inconspicuous crystallization on its surface demonstrates that Rg3 was well dissolved and evenly loaded in it. The sol-gel transition study of the hydrogel confirms that it is in liquid form at room temperature, and turns to gel formation when applied on the surface of perianal ulcer, a kind of common post-surgical complication of perianal disease [21,22]. The perianal tissue edema, bleeding, and contamination often lead to severe inflammation, generating ulceration and delayed wound recovery [6,22]. By completely covering the wound area with the porous Rg3-loaded hydrogel, the aim is to facilitate the wound healing process of perianal ulcers.

The biocompatibility and biodegradability of polymer-based materials are vital for in vivo applications [23,24]. The degradation study shows that most of the hydrogel can be degraded in 5 weeks without causing serious tissue edema or inflammatory responses. The study proves that the synthesized gel is biocompatible and biodegradable. Sustained drug release to the target sites is essential for wound healing [3]. The drug release study was performed by detecting the released Rg3 from H-Rg3 immersed in PBS solution or elastase solution (0.02 mg/mL). Elastase is a common pancreatic enzyme that digests fibrous glycoprotein in vivo. The in vitro degradation and drug release studies in elastase solution can mimic the in vivo polymer degradation properties and drug release profiles [25,26]. H-Rg3 can be degraded quickly in the presence of elastase and more loaded agents can be released. As a result, the released Rg3 was more in Elastase group than that in PBS group at 120 h. Moreover, a fast burst release of agents can be found in both groups, which can be attributed to the porous structure and large surface area of hydrogel, the distribution of agents near the hydrogel surface, and quick degradation of the gel [27,28]. The in vitro cytotoxicity study showed that the hydrogel had no effect on the survival rate of murine skin fibroblasts L929 and may be used for ulcer healing promotion.

The perianal ulcer rat model was established to evaluate the treatment efficacy of H-Rg3 towards perianal ulcer. The ulceration almost disappeared in H-Rg3 and Lidocaine groups at 15 days. H group also showed lower residual wound area rate than Control group (***$P < 0.001$). That is possibly sparked by the functions of the gel: maintaining the moist environment of the wound, restraining cell death, and boosting collagen deposition and epidermal migration [29,30]. The porous structure of our hydrogel can also propel the oxygen transmission and the communication of nutrients and other molecules for ulcer healing promotion [31–33]. It is seminal to curb the inflammation process for ulcer recovery as it goes with wound deterioration [33,34]. IL-1 and IL-6, common but essential inflammatory factors during inflammation, swell the formation of oxygen radicals and the permeability of capillaries [35,36]. Blood IL-1 values were the lowest in H-Rg3 group than that in the other four groups at 6 days and 15 days. For IL-6, H-Rg3 and Lidocaine groups showed the lowest levels compared with other groups. Our results demonstrate that Rg3 released from the hydrogel can downregulate the expressions of inflammatory factors, inhibiting the systematical inflammation. VEGF is a kind of growth factor that promotes angiogenesis for wound healing [37,38]. In our study, there was significant difference of blood VEGF values between H-Rg3 group and the other groups. This indicates that Rg3 could promote VEGF expression, thus increasing angiogenesis and benefiting wound healing.

To further evaluate the treatment efficacy of H-Rg3 for perianal ulcers, histopathology analysis of the ulcer tissues was performed at 6 days and 15 days after treatment. The histopathology results showed that the wound healing process was initiated in H-Rg3 and Lidocaine groups with the formation of fibrous tissue at 6 days post treatment. The perianal ulcer healed well with abundant fibrous tissues and angiogenesis in H-Rg3 group at 15 days post treatment. The local inflammatory cells count results also showed that H-Rg3 possessed the best inflammation inhibition effect among all the groups. The results indicated that the Rg3-loaded hydrogel could curb both systematic inflammation and the inflammatory responses in local ulceration tissues, processing satisfied anti-inflammation effects that benefited perianal ulceration healing. As a key process for wound contraction and scar formation during ulceration healing, collagen deposition was assessed by Masson staining of the perianal ulcer tissues with the outcome of slight stain. Moreover, semiquantitative analysis of the collagen expression levels was calculated by Image J software. H-Rg3 showed the most collagen deposition effect in the ulcer tissues compared with the other groups. The results showed that Rg3-loaded hydrogel could promote collagen deposition, facilitating the healing of the perianal ulcer.

The immunohistochemical analyses further demonstrate the treatment mechanism of H-Rg3 for perianal ulcers. TNF-α was a key inflammatory factor that could associate many immune responses and induce the formation of IL-1 and IL-6, thus promoting the inflammation process [39]. There was statistical difference in TNF-α expression between H-Rg3 group and H group at 6 days and 15 days post treatment. This demonstrated that H-Rg3 possessed better local inflammation inhibition effect than H, which can be attributed to the anti-inflammation activity of Rg3. Furthermore, TNF-α expression was less in H-Rg3 group than that in free Rg3 group. This is possibly sparked by the fact that the hydrogel can maintain a moist environment, increase the communication of oxygen and other nutrients, and inhibit wound infection [19]. Ki-67 and CD31 immunohistochemical staining was performed to analyze the proliferation of nucleated cells and angiogenesis effect of H-Rg3 for perianal ulcer [40,41]. H-Rg3 group showed the most Ki-67 and CD31 levels compared with other groups. Our results demonstrated that H-Rg3 promoted the proliferation of nucleated cells and vascularization which could further benefit wound healing. ERK signal pathway regulates many physiological processes during wound healing, such as cell growth, proliferation, differentiation, and apoptosis [42]. Activation of ERK signal pathway can accelerate the healing process of wound. Immunohistochemical staining of ERK1/2 demonstrated that H-Rg3 had the most ERK activation effect compared with other treatment methods. H-Rg3 can enhance the healing of perianal ulcer by upregulation of ERK pathway. NF-κB plays an important role in facilitating pro-inflammatory gene expression [42]. Therefore, down-regulation of NF-κB leads to inflammation inhibition effect. In this study, H-Rg3 decreased the expression of NF-κB, thus preventing the inflammatory responses for better perianal ulcer treatment.

Fig. 5. Immunohistochemical analysis of perianal ulcers in different groups at 6 days and 15 days after treatment. (A) Immunohistochemical staining of TNF-α, Ki-67, CD31, ERK1/2, and NF-κB of perianal ulcer tissues. Relative positive area of (B) TNF-α, (C) Ki-67, (D) CD31, (E) ERK1/2, and (F) NF-κB. Scale bars = 100 μm. The images in the red squares are the enlargement of the images in the corresponding red dotted squares.

In this study, the best healing effect of the perianal ulcer was observed in H-Rg3. It exceeded Lidocaine and free Rg3 in curbing inflammation and boosting fibrous deposition and vascularization, working best in perianal ulcer healing and scar formation than other methods. Furthermore, the wound healing effect of H could be explained by the features and function of the hydrogel discussed above. As a result, the hydrogel used in this study could benefit the healing of perianal ulcer. Through sustained releasing Rg3 from the hydrogel, the inflammatory responses can be inhibited, the collagen deposition, nuclear cell proliferation, and tissue vascularization can be increased, and the ERK signal pathway can be activated. Therefore, the combination of hydrogel and Rg3 provided a satisfactory perianal ulcer healing effect.

Declaration of competing interest

The authors declare that there are no conflicts of interest.

Acknowledgement

This study was supported by Youth Program of the National Natural Science Foundation of China (#32000953), Department of Finance of Jilin Province (#3D5197434429), Health Commission of Jilin Province (2021LC019), and the Education Project of Jilin University (#419070600046 and 45121031D024). We thank Prof. Peng Zhao for helping us revise this study.

References

[1] Nosrati H, Aramideh Khouy R, Nosrati A, Khodaei M, Banitalebi-Dehkordi M, Ashrafi-Dehkordi K, Sanami S, Alizadeh Z. Nanocomposite scaffolds for accelerating chronic wound healing by enhancing angiogenesis. J Nanobiotechnol 2021;19(1):1.
[2] Veith AP, Henderson K, Spencer A, Sligar AD, Baker AB. Therapeutic strategies for enhancing angiogenesis in wound healing. Adv Drug Deliv Rev 2019;146:97–125.
[3] Xue M, Zhao R, March L, Jackson CJ. Dermal fibroblast heterogeneity and its contribution to the skin repair and regeneration. Adv Wound Care 2021;11(2):87–107.
[4] Rong X, Li J, Yang Y, Shi L, Jiang T. Human fetal skin-derived stem cell secretome enhances radiation-induced skin injury therapeutic effects by promoting angiogenesis. Stem Cell Res Ther 2019;10(1):383.
[5] Rong X, Chu W, Zhang H, Wang Y, Qi X, Zhang G, Wang Y, Li C. Antler stem cell-conditioned medium stimulates regenerative wound healing in rats. Stem Cell Res Ther 2019;10(1):326.
[6] Xu X, Li X, Zhang L, Liu Z, Pan Y, Chen D, Bin D, Deng Q, Sun Y, Hoffman RM, Yang Z, Yuan H. Enhancement of wound healing by the traditional Chinese medicine herbal mixture Sophora flavescens in a rat model of perianal ulceration. Vivo 2017;31(4):543–9.
[7] Sugimoto T, Tsunoda A, Kano N, Kashiwagura Y, Hirose K-i, Sasaki T. A randomized, prospective, double-blind, placebo-controlled trial of the effect of diltiazem gel on pain after hemorrhoidectomy. World J Surg 2013;37(10):2454–7.
[8] Homaeigohar S, Boccaccini AR. Antibacterial biohybrid nanofibers for wound dressings. Acta Biomater 2020;107:25–49.
[9] Miguel SP, Sequeira RS, Moreira AF, Cabral CSD, Mendonca AG, Ferreira P, Correia IJ. An overview of electrospun membranes loaded with bioactive molecules for improving the wound healing process. Eur J Pharm Biopharm 2019;139:1–22.
[10] Kim HS, Sun X, Lee J-H, Kim H-W, Fu X, Leong KW. Advanced drug delivery systems and artificial skin grafts for skin wound healing. Adv Drug Deliv Rev 2019;146:209–39.
[11] Vijayakumar V, Samal SK, Mohanty S, Nayak SK. Recent advancements in biopolymer and metal nanoparticle-based materials in diabetic wound healing management. Int J Biol Macromol 2019;122:137–48.
[12] Sturkie EK, Moore CR, Caulfield CA, Schmid E, Lachiewicz AM, Stephens JR. Frequency and yield of blood cultures for observation patients with skin and soft tissue infections. Am J Emerg Med 2021;44:161–5.
[13] Sun M, Ye Y, Xiao L, Duan X, Zhang Y, Zhang H. Anticancer effects of ginsenoside Rg3 (review). Int J Mol Med 2017;39(3):507–18.
[14] Zhang K, Liu Y, Wang C, Li J, Xiong L, Wang Z, Liu J, Li P. Evaluation of the gastroprotective effects of 20 (S)-ginsenoside Rg3 on gastric ulcer models in mice. J Ginseng Res 2019;43(4):550–61.
[15] Lim T-G, Lee CC, Dong Z, Lee KW. Ginsenosides and their metabolites: a review of their pharmacological activities in the skin. Arch Dermatol Res 2015;307(5):397–403.
[16] Qiu R, Qian F, Wang X, Li H, Wang L. Targeted delivery of 20(S)-ginsenoside Rg3-based polypeptide nanoparticles to treat colon cancer. Biomed Microdevices 2019;21(1):18.
[17] Cheng L, Sun X, Hu C, Jin R, Sun B, Shi Y, Cui W, Zhang Y. In vivo early intervention and the therapeutic effects of 20(S)-Ginsenoside Rg3 on hypertrophic scar formation. PLoS One 2014;9(12):e113640.
[18] Cheng L, Sun X, Hu C, Jin R, Sun B, Shi Y, Zhang L, Cui W, Zhang Y. In vivo inhibition of hypertrophic scars by implantable ginsenoside-Rg3-loaded electrospun fibrous membranes. Acta Biomater 2013;9(12):9461–73.
[19] Bai H, Kyu-Cheol N, Wang Z, Cui Y, Liu H, Liu H, Feng Y, Zhao Y, Lin Q, Li Z. Regulation of inflammatory microenvironment using a self-healing hydrogel loaded with BM-MSCs for advanced wound healing in rat diabetic foot ulcers. J Tissue Eng 2020;11. 2041731420947242.
[20] Liu H, Zhu X, Guo H, Huang H, Huang S, Huang S, Xue W, Zhu P, Guo R. Nitric oxide released injectable hydrogel combined with synergistic photothermal therapy for antibacterial and accelerated wound healing. Appl Mater Today 2020;20:100781.
[21] Pescatori M. Closed vs. open hemorrhoidectomy: associated sphincterotomy and postoperative bleeding. Dis Colon Rectum 2000;43(8):1174–5.
[22] Sugimoto T, Tsunoda A, Kano N, Kashiwagura Y, Hirose K, Sasaki T. A randomized, prospective, double-blind, placebo-controlled trial of the effect of diltiazem gel on pain after hemorrhoidectomy. World J Surg 2013;37(10):2454–7.
[23] Su T, Yang B, Gao T, Liu T, Li J. Polymer nanoparticle-assisted chemotherapy of pancreatic cancer. Therap Adv Med Oncol 2020;12. 1758835920915978.
[24] Qiu R, Sun D, Bai Y, Li J, Wang L. Application of tumor-targeting peptide-decorated polypeptide nanoparticles with doxorubicin to treat osteosarcoma. Drug Deliv 2020;27(1):1704–17.
[25] Li J, Xu W, Li D, Liu T, Zhang YS, Ding J, Chen X. Locally deployable nanofiber patch for sequential drug delivery in treatment of primary and advanced orthotopic hepatomas. ACS Nano 2018;12(7):6685–99.
[26] Li J, Xu W, Chen J, Li D, Zhang K, Liu T, Ding J, Chen X. Highly bioadhesive polymer membrane continuously releases cytostatic and anti-inflammatory drugs for peritoneal adhesion prevention. ACS Biomater Sci Eng 2018;4(6):2026–36.
[27] Qiu H, Guo H, Li D, Hou Y, Kuang T, Ding J. Intravesical hydrogels as drug reservoirs. Trends Biotechnol 2020;38(6):579–83.
[28] Zheng Y, Cheng Y, Chen J, Ding J, Li M, Li C, Wang J-c, Chen X. Injectable hydrogel-microsphere construct with sequential degradation for locally synergistic chemotherapy. ACS Appl Mater Interfaces 2017;9(4):3487–96.
[29] Liu H, Wang C, Li C, Qin Y, Wang Z, Yang F, Li Z, Wang J. A functional chitosan-based hydrogel as a wound dressing and drug delivery system in the treatment of wound healing. RSC Adv 2018;8(14):7533–49.
[30] Boateng JS, Matthews KH, Stevens HNE, Eccleston GM. Wound healing dressings and drug delivery systems: a review. J Pharmaceut Sci 2008;97(8):2892–923.
[31] Yao Y, Zhang A, Yuan C, Chen X, Liu Y. Recent trends on burn wound care: hydrogel dressings and scaffolds. Biomater Sci 2021;9(13):4523–40.
[32] Sulastri E, Lesmana R, Zubair MS, Elamin KM, Wathoni N. A comprehensive review on ulvan based hydrogel and its biomedical applications. Chem Pharmaceut Bull 2021;69(5):432–43.
[33] Hawthorne B, Simmons JK, Stuart B, Tung R, Zamierowski DS, Mellott AJ. Enhancing wound healing dressing development through interdisciplinary collaboration. J Biomed Mater Res B Appl Biomater 2021;109(12):1967–85.
[34] Xu Z, Liang B, Tian J, Wu J. Anti-inflammation biomaterial platforms for chronic wound healing. Biomater Sci 2021;9(12):4388–409.
[35] Ostadkarampour M, Putnins EE. Monoamine oxidase inhibitors: a review of their anti-inflammatory therapeutic potential and mechanisms of action. Front Pharmacol 2021;12:676239.
[36] Rose-John S. Therapeutic targeting of IL-6 trans-signaling. Cytokine 2021;144:155577.
[37] Radovic K, Brkovic B, Roganovic J, Ilic J, Milic Lemic A, Jovanovic B. Salivary VEGF and post-extraction wound healing in type 2 diabetic immediate denture wearers. Acta Odontol Scand 2021;80(1):9–14.
[38] Brinkmann A, Winkelmann K, Kaeckenmeister T, Roider J, Klettner A. Effect of long-term anti-VEGF treatment on viability and function of RPE cells. Curr Eye Res 2021;47(1):127–34.
[39] Chung M-Y, Jung SK, Lee H-J, Shon DH, Kim H-K. Ethanol extract of sarcodon asparatus mitigates inflammatory responses in lipopolysaccharide-challenged mice and murine macrophages. J Med Food 2015;18(11):1198–206.
[40] Xie P, Jia S, Tye R, Xu W, Zhong A, Hong SJ, Galiano RD, Mustoe TA. Topical administration of oxygenated hemoglobin improved wound healing in an ischemic rabbit ear model. Plast Reconstr Surg 2016;137(2):534–43.
[41] Maeda T, Yamamoto T, Imamura T, Tsuboi R. Impaired wound healing in bleomycin-induced murine scleroderma: a new model of wound retardation. Arch Dermatol Res 2016;308(2):87–94.
[42] Chakrabarti S, Mazumder B, Rajkonwar J, Pathak MP, Patowary P, Chattopadhyay P. bFGF and collagen matrix hydrogel attenuates burn wound inflammation through activation of ERK and TRK pathway. Sci Rep 2021;11(1):3357.